0026-895X/02/6105-964–973$7.00
MOLECULAR PHARMACOLOGY
Copyright © 2002 The American Society for Pharmacology and Experimental Therapeutics
Mol Pharmacol 61:964–973, 2002

Vol. 61, No. 5
1471/981200
Printed in U.S.A.

Three-Dimensional Quantitative Structure-Activity Relationships of Inhibitors of P-Glycoprotein

SEAN EKINS, RICHARD B. KIM, BRENDA F. LEAKE, ANNE H. DANTZIG, ERIN G. SCHUETZ, LU-BIN LAN, KAZUTO YASUDA, ROBERT L. SHEPARD, MARK A. WINTER, JOHN D. SCHUETZ, JAMES H. WIKEL, and STEVEN A. WRIGHTON

Lilly Research Laboratories, Eli Lilly and Co., Lilly Corporate Center, Indianapolis, Indiana (S.E., A.H.D., R.L.S., M.A.W., J.H.W., S.A.W.); Division of Clinical Pharmacology, Vanderbilt University, Nashville, Tennessee (R.B.K., B.F.L.); Department of Pharmaceutical Sciences, St. Jude Children's Research Hospital, Memphis, Tennessee (E.G.S., L.-B.L., K.Y., J.D.S.)

Received November 2, 2001; accepted February 13, 2001

This article is available online at http://molpharm.aspetjournals.org

ABSTRACT

P-glycoprotein (P-gp) is an efflux transporter involved in limiting the oral bioavailability and tissue penetration of a variety of structurally divergent molecules. A better understanding of the structural requirements of modulators of P-gp function will aid in the design of therapeutic agents. Toward this goal, three-dimensional quantitative structure-activity relationship (3D-QSAR) models were generated using in vitro data associated with inhibition of P-gp function. Several approaches were undertaken with multiple iterations, yielding Catalyst 3D-QSAR models being able to qualitatively rank-order and predict IC_{50} values for P-gp inhibitors excluded from the model in question. The success of these validations suggests that a P-gp pharmacophore for 27 inhibitors of digoxin transport in Caco-2 cells consisted of four hydrophobes and one hydrogen bond acceptor. A second pharmacophore generated with 21 inhibitors of vinblastine binding to plasma membrane vesicles derived from CEM/VLB_{100} cells contained three ring aromatic features and one hydrophobic feature. A third pharmacophore generated with 17 inhibitors of vinblastine accumulation in P-gp expressing LLC-PK1 cells contained four hydrophobes and one hydrogen bond acceptor. A final pharmacophore was generated for inhibition of calcein accumulation in P-gp expressing LLC-PK1 cells and found to contain two hydrophobes, a ring aromatic feature, and a hydrogen bond donor. The similarity of features for the pharmacophores of P-gp inhibitors of digoxin transport and vinblastine binding suggest some commonality in their binding sites. Utilization of such models may prove to be of value for prediction of molecules that may modulate one or more P-gp binding sites.

The ATP-binding cassette efflux transporter P-glycoprotein (P-gp) is a large membrane-bound protein initially noted to be present in certain malignant cells associated with the multidrug resistance (MDR) phenomenon (Wandell et al., 1999a). However, P-gp is normally expressed at many physiological barriers, including the intestinal epithelium, canalicular domain of hepatocytes, brush border of proximal tubule cells, and capillary endothelial cells in the central nervous system (Wandell et al., 1999a). Expression of P-gp in such locations results in reduced oral drug absorption and enhanced renal and biliary excretion of substrate drugs. Moreover, P-gp expression at the blood-brain barrier is a key factor in the limited central nervous system entry of many drugs. The expressed level of P-gp, as well as altered functional activity of the protein due to genetic variability in the *MDR1* gene, seems to also impact the ability of this transporter to influence the disposition of drug substrates (Hoffmeyer et al., 2000).

In terms of P-gp structure-activity relationship, photoaffinity experiments have been valuable in defining the cyclosporin binding site in hamster P-gp (Demeule et al., 1998) and indicating that trimethoxybenzoylyohimbine (TMBY) and verapamil bind to a single or overlapping sites in a human leukemic cell line (Shepard et al., 1998). Additional studies have shown that TMBY is a competitive inhibitor of vinblastine binding to P-gp (Dantzig et al., 1996). The P-gp modulator LY335979 has been shown to competitively block vinblastine binding (Dantzig et al., 1996), whereas vinblastine itself can competitively inhibit verapamil stimulation of P-gp–ATPase (Shepard et al., 1998). With the growth in knowledge derived from these and other studies using different probes and cell systems, it would be valuable to use structural information to define whether unrelated mole-

This work was supported in part by United States Public Health Service grant GM31304 (to R.B.K.) and National Institutes of Health grant ES08658 (to E.S.).

ABBREVIATIONS: P-gp, P-glycoprotein; MDR, multidrug resistance; TMBY, trimethoxybenzoylyohimbine; 3D-QSAR, 3-dimensional structure activity relationship; CoMFA, comparative molecular field analysis; AM, acetoxymethyl ester; LY335979, 4-(1,1-difluoro-1,1a,6,10b-tetrahydrodibenzo[*a*,*e*]cyclopropa[*c*]cyclohepten-6-yl)-[(5-quinolinyloxy)methyl]-1-piperazineethanol.

cules are likely to interact with P-gp. Early studies using such P-gp modulators as verapamil, reserpine, 18-epireserpine, and TMBY showed that they could be aligned suggesting the importance of aromatic rings and a basic nitrogen atom in P-gp modulation (Pearce et al., 1989; Pearce et al., 1990). A subsequent, more extensive study with 232 phenothiazines and structurally related compounds indicated that molecules with a carbonyl group that is part of an amide bond with a tertiary amine, were active P-gp inhibitors (Ramu and Ramu, 1992). A model built with 21 molecules of various structural classes that modulate P-gp ATPase activity suggested that these molecules competed for a single binding site (Borgnia et al., 1996). Similarly, 19 propafenone type P-gp inhibitors were then used to confirm the requirement for a carbonyl oxygen, suggested to form a hydrogen bond with P-gp (Chiba et al., 1996). Others have used MULTICASE to determine important substructural features like CH_2-CH_2-N-CH_2-CH_2 (Klopman et al., 1997), and linear discriminant analysis with topological descriptors (Bakken and Jurs, 2000). In 1997, the first 3D-QSAR analysis of phenothiazines and related drugs known to be P-gp inhibitors was described previously (Pajeva and Wiese, 1997). This was followed by Hansch-type QSAR studies with propafenone analogs (Salem et al., 1998; Tmej et al., 1998), CoMFA studies of phenothiazines and related drugs (Pajeva and Wiese, 1998a), CoMFA studies of propafenone analogs (Pajeva and Wiese, 1998b), and simple regression models of propafenone analogs (Ecker et al., 1999; Schmid et al., 1999). These latter models confirmed the relevance of hydrogen bond acceptors and the basic nitrogen for inhibitors (Ecker et al., 1999; Schmid et al., 1999) and multiple hydrogen bond donors in substrates 2.5 to 4.6 Å apart (Seelig, 1998). One study using a diverse array of inhibitors on P-gp ATPase activity noted that size of the molecular surface, polarizability, and hydrogen bonding had the largest impact on the ATPase activity (Osterberg and Norinder, 2000). A number of computational approaches and models of P-gp have yielded useful information that is usually derived from a series of structurally related molecules. A recent example suggested P-gp inhibitors with high lipophilicity and polarizability were more likely to be high-affinity ligands for the verapamil-binding site (Neuhoff et al., 2000). However, some complexity arises if one considers more structurally diverse molecules, because they may bind to different sites within P-gp. This hypothesis derives from experimental results describing a complex behavior for P-gp such that co-operative, competitive, and noncompetitive interactions between modulators may occur (Ayesh et al., 1996), indicative of multiple binding sites within P-gp (Dey et al., 1997; Scala et al., 1997; Shapiro and Ling, 1997).

So far, a specific model(s) addressing the individual P-gp binding site(s) using a diverse array of inhibitors have not been described. Previously, we have used computational approaches to predict substrate and inhibitor interactions with specific cytochromes P450 (Ekins et al., 1999, 2000) to produce 3D pharmacophores to aid in drug design from a metabolism perspective and assist in increasing the quality of potential drug candidates. Accordingly, the present study used a similar computational approach to model in vitro data derived from structurally diverse inhibitors of digoxin transport in Caco-2 cells, vinblastine and calcein accumulation in P-gp expressing LLC-PK1 (L-MDR1) cells, or vinblastine binding in vesicles derived from CEM/VLB_{100} cells. The findings described in this report using different probes and cell systems representative of those commonly used serves as an initial step toward characterization and prediction of P-gp–mediated drug transport both in vitro and in silico.

Experimental Procedures

Materials. [^{3}H]Digoxin (15 Ci/mmol) was supplied by PerkinElmer Life Sciences (Boston, MA), calcein AM was from Molecular Probes (Eugene, OR), and all ergot alkaloids were from Sigma/RBI (Natick, MA). All other chemical and reagents, unless stated otherwise, were obtained from Sigma-Aldrich Research (St. Louis, MO) and were of the highest quality available.

Cell Lines. LLC-PK1 pig kidney epithelial cells and derivative cells containing human *MDR1* (L-MDR1) were generously provided by Dr. Alfred Schinkel (The Netherlands Cancer Institute, Amsterdam, The Netherlands) and cultured as described previously (Schinkel et al., 1995).

Transport in Caco-2 Cells. Cells were plated on Transwell (Costar, Cambridge, MA) filters and grown under identical conditions as described previously (Kim et al., 1998). About 1 to 2 h before the start of the transport experiments, the medium in each compartment was replaced with a serum-free medium (OptiMEM; Invitrogen, Carlsbad, CA). Then, the medium in each compartment was replaced with 700 μl of serum-free medium (OptiMEM), with [^{3}H]digoxin (5 μM) in either the apical or the basal compartment. The amount of the drug appearing in the opposite compartment after 1, 2, 3, and 4 h was measured in 25-μl aliquots taken from each compartment.

Inhibition of P-gp–mediated transport by Caco-2 cells was determined in a similar manner after the addition of the putative inhibitor to both the apical and basal compartments, and using 5 μM [^{3}H]digoxin as the P-gp substrate. Complete inhibition of P-gp–mediated transport would be expected to result in the loss of the digoxin basal-to-apical (B→A) versus apical-to-basal (A→B) transport difference. Accordingly, percentage inhibition was estimated by this equation: Degree of inhibition = $[1 - [(i_{B\rightarrow A} - i_{A\rightarrow B}) / (a_{B\rightarrow A} - a_{A\rightarrow B})]] \times 100\%$, where i and a are the percentages of digoxin transport in the presence and absence of the putative inhibitor, according to the direction of transport. Values estimated at each time point were averaged because digoxin transport seemed to be linear with respect to time. Controls for digoxin transport in the absence of any inhibitor (two wells per plate) were included on every plate (12 wells). IC_{50} values were estimated from the Hill equation using the computer program Prism (GraphPad Software Inc., San Diego, CA), and the presented data represent results obtained from at least three preparations on different days.

Aliquots (25 μl) of the compartmental buffer solution containing radiolabeled digoxin were analyzed by liquid scintillation counting (1219 Rackbeta LSC; LKB-Wallace, Gaithersburg MD), after the addition of 5 ml of ScintiVerse BD (Fisher Scientific, Fairlawn, NJ) scintillation fluid.

Plasma Membrane Preparation. Plasma membranes of CEM/VLB_{100} cells were prepared by nitrogen cavitation and differential centrifugation. A total of 1 to 3.5 $\times$ 10^9 cells in logarithmic growth phase were centrifuged and washed as reported by Lever (1977). The pellet was resuspended at ~3 $\times$ 10^7 cells/ml in 0.2 mM $CaCl_2$, 0.25 M sucrose, 0.02 mM phenylmethylsulfonyl fluoride, and 0.01 M Tris-HCl, pH 7.4. Cells were disrupted by nitrogen cavitation (Parr Instrument Co., Moline, IL) at 175 psi. After removal of nuclei and unbroken cells by centrifugation, 1 mM EDTA was added to the supernatant and centrifuged at 9000*g* for 20 min to remove mitochondria. The resulting supernatant was layered onto a 35% sucrose gradient and centrifuged at 16,000*g* for 1 h as described previously (Lever, 1977). Membranes collected at the interface were subsequently pelleted at 100,000*g* for 1 h, resuspended in 0.20 M sucrose

and 0.05 M Tris-HCl, pH 7.4, passed through a 25-gauge needle, and stored up to 2 months at −70°C. Protein was determined with bicinchoninic acid and bovine serum albumin as the standard (Smith et al., 1985). The orientation of the membrane vesicles was estimated to be 95% inside-out as determined by the activity of Na^+,K^+-ATPase measured in sealed and unsealed lyophilized vesicles.

Equilibrium Binding. A rapid filtration method was used to determine equilibrium binding to plasma membranes. Routinely, CEM/VLB_{100} plasma membranes (~20 μg of protein) were incubated in 200 μl of total volume of 0.20 M sucrose, 3 mM ATP, 1 mM $MgCl_2$, and 0.05 M Tris-HCl, pH 7.4 (buffer A) containing 0.1% bovine serum albumin and 40 nM [^{3}H]vinblastine. The assay mixture was incubated at 25°C soaked overnight with 3% bovine serum albumin in 1-ml, 96-well polystyrene plates (Beckman Coulter, Fullerton, CA). After 150 min, plasma membranes were aspirated onto membrane filters (GF/C; Brandel, Inc., Gaithersburg, MD), soaked overnight in 10% FBS, 0.02 M sucrose, and 0.01 M Tris-HCl, pH 7.4, with a 48-channel cell harvester (Brandel) and rapidly washed five times with 1 ml of ice-cold buffer A. The wash buffer contained the same concentration of the indicated nucleotide as in the incubation condition. IC_{50} values were determined. For vinblastine, the total binding was corrected for nonspecific binding measured in the presence of 400 μM vinblastine. Unless noted otherwise, values are the mean of triplicate determinations.

Calcein-AM Fluorometry Assay. This was performed as described previously (Tiberghein and Loor, 1996). LLC-PK1 and L-MDR1 cells were cultured at 100,000 cells/well in phenol-free medium in Costar 96-well plates on day zero. We carried out the inhibitor studies at the K_m value of calcein AM for P-gp in L-MDR1 cells [determined to be ~1 μM (Dr. Ryan Yates, University of Tennessee, personal communication)]. On day 1 medium was removed and the well washed once with 200 μl of Hanks' buffered saline (Invitrogen). Hanks' buffered saline (100 μl) with or without 2× reverser was added and the cells incubated for 30 min at 37°C. Then, 100 μl of Hanks buffer containing calcein-AM (2 μM in dimethyl sulfoxide) (Molecular Probes, Eugene OR), was added to reach a final calcein-AM plate concentration of 1 μM and the microplates were analyzed with a fluorescence microplate reader (Cytofluor 2350; Millipore, Bedford, MA) with excitation and emission wavelengths set at 485 nm and 530 nm, respectively (calcein excitation, 494 nm; emission, 517 nm). The plate was scanned at 3-min intervals repeated 11 times over 30 min at 25°C. For each drug, simultaneous treatment of LLC-PK1 cells allowed determination of whether there were nonspecific effects of modulators on, for example, calcein fluorescence or esterase activity. Each data point was determined by averaging at least two independent experiments using three wells per cell line per treatment. The data were fitted using a modified form of the Michaelis-Menten equation (Lan et al., 1996): $Di = Dr + (Ds - Dr) \times (C/K_i + C)$, where Di is the measured amount of calcein accumulated at the reverser concentration C (inhibitor), whereas Ds and Dr are the amount of calcein accumulation for fully reversed (equivalent to sensitive) cells and resistant cells, respectively. K_i is the reverser concentration required for half-reversal of calcein accumulation. The quantity (Ds − Dr) is the increment in calcein accumulation brought about by the action of a maximal concentration of the reverser.

[^{3}H]Vinblastine Accumulation in LLC-PK1 and L-MDR1 Cells. To assess drug uptake we used a modification of the procedure described previously (Schuetz and Schuetz, 1993; Lan et al., 1996). Briefly, cultured cells were placed in media containing 2 μM ^{3}H and unlabeled vinblastine in the presence or absence of various concentrations of inhibitor and incubated at 37°C with 5% CO_2 for 1 h. Individual dishes were washed three times with ice-cold phosphate-buffered saline, cells scraped to harvest, resuspended in phosphate-buffered saline, sonicated, and analyzed for radioactivity using a scintillation counter. Each data point was assayed in duplicate and the experiment repeated three times. The K_i was calculated using a modified form of the Michaelis-Menten equation (Lan et al., 1996).

Molecular Modeling. The computational molecular modeling studies were carried out using Silicon Graphics Octane and O_2 workstations. Molecular structures were used as SMILES (Simplified Molecular Input Line Entry System) string format (Weininger, 1988) or imported from the ISIS MDDR-3D database (version 2000.2; MDL Information Inc., San Leandro, CA).

Modeling with Catalyst. Briefly, models were constructed using Catalyst version 4.5 (Molecular Simulations, San Diego, CA) after importing the molecular structures (LY molecules shown in Fig. 1) used in the in vitro studies and from the literature (Wandell et al., 1999a; Neuhoff et al., 2000). The three-dimensional molecular structures were generated as described previously for cytochrome P450s (Ekins et al., 1999). The data from each assay for P-gp inhibition was each treated as follows. For each molecule in either the training or test sets the number of conformers generated using the 'best' functionality for each inhibitor was limited to a maximum number of 255, with an energy range of 20 kcal/mol. Ten hypotheses were generated using these conformers for each of the molecules in the training sets and the IC_{50} or K_i values, after selection of the following features for the inhibitors: hydrogen bond donor, hydrogen bond acceptor, hydrophobic, and ring aromatic. After assessing all 10 hypotheses generated, the lowest energy cost hypothesis was considered the best as this possessed features representative of all the hypotheses and had the lowest total cost.

The quality of the structure activity correlation between the estimated and observed activity values was estimated by means of an r^2 value. Statistical significance of the retrieved hypothesis was verified by permuting (randomizing) the response variable 10 times (i.e., the activities and structures of the training set compounds were mixed 10 times), so that each value was no longer assigned to the original molecule, and the catalyst hypothesis generation procedure was repeated. The total energy cost of the generated pharmacophores can be calculated from the deviation between the estimated activity and the observed activity, combined with the complexity of the hypothesis (i.e., the number of pharmacophore features). A null hypothesis can also be calculated that presumes that there is no relationship in the data and the experimental activities are normally distributed about their mean. Hence, the greater the difference between the energy cost of the generated hypothesis and the energy cost of the null hypothesis, the less likely it is that the hypothesis reflects a chance correlation.

Validation of the Catalyst Models. The test sets contained molecules with IC_{50} or K_i values not included in the initial training sets as described previously (common molecules were excluded). These test set molecules were fit by the fast-fit algorithm to the respective catalyst models to predict an IC_{50} or K_i value as described previously for cytochromes P450 (Ekins et al., 1999). Fast-fit refers to the method of finding the optimum fit of the substrate to the hypothesis among all the conformers of the molecule without performing an energy minimization on the conformers of the molecule.

Statistical Evaluation of Test Set Predictions. Observed and predicted inhibition data were graphed (data not shown) and fit using Excel 97 (Microsoft, Redmond, WA) to generate an r^2 value. This data was also analyzed using the nonparametric Spearman's Rho test available in JMP 4.0.2 (SAS Institute Inc., Cary, NC). This test represents a correlation coefficient computed on the ranks of the data values and not the values themselves.

Results

To gain an understanding of the binding sites of P-gp, the present study used a computational approach to model in vitro data derived using structurally diverse inhibitors. Inhibition of digoxin transport in Caco-2 cells, vinblastine, and calcein accumulation in P-gp expressing LLC-PK1 (L-MDR-1) cells as well as vinblastine binding in vesicles derived from CEM/VLB100 cells were all assessed because they

represent widely used chemical probes and cell systems. The catalyst pharmacophore approach generated models of the position of important ligand features in three-dimensional space that may ultimately relate to features within P-gp. These models were achieved by assessing multiple conformations of each ligand alongside the experimental inhibition data (Ekins et al., 2000). The result is a computational model that can be used to predict how other molecules might inhibit P-gp solely by providing the structure to the software, which then attempts to fit the numerous conformations of the molecule as close to the centroids of the pharmacophore features as possible. Pharmacophore models built with each data set were tested with the other results individually after omitting molecules that were already in the respective training set. These assessments were used to provide an idea of how well each model ranked external observations. These results were then combined to provide an appreciation of the similarities and differences for the model derived for each substrate probe and in vitro system.

A pharmacophore for inhibition of digoxin transport by P-gp in Caco-2 cells (Fig. 2) generated with 27 diverse molecules (Table 1) consisted of four hydrophobes (contiguous set of surface accessible atoms not adjacent to any concentration of charge) and 1 hydrogen bond acceptor (nonbasic amines that have a lone pair, sp or sp2 nitrogens, sp3 oxygens or sulfurs, and sp2 oxygens). This model possessed an observed versus predicted correlation of $r^2 = 0.77$ for the training set. The total energy cost of this pharmacophore was 127.9 units, considerably lower than the null cost (172.1 units). Randomizing the activity and structures of molecules in the digoxin model 10 times resulted in a lower r^2 value of 0.43 for the training set. The most potent P-gp inhibitor in the model is LY335979, which fits closely to the five features in the model (Fig. 3). This model was used to predict the inhibitory potential of nineteen molecules with data excluded from the training set (Table 2). On the whole, these predictions are reasonable if one takes into account that a number of observed values are actually categorized (that is greater or less than a certain value or given as a range of values such as 10–100 μM). The model poorly predicts FK506, colchicine, and PSC833 because the predictions are outside of 1 log unit compared with the experimental value. The digoxin inhibition pharmacophore was further evaluated using a second test set of molecules with known IC_{50} data generated for inhibitors of vinblastine binding in vesicles of CEM/VLB_{100} (Table 3). The pharmacophore model for inhibition of digoxin transport poorly predicts 4 of 19 molecules (verapamil and LY335979 were excluded because they were included in the training set of the model) using the log unit cut-off criteria. However, on the whole, this model is able to differentiate correctly the best inhibitors for vinblastine binding to P-gp from the poorest inhibitors. When these predictions are analyzed statistically, an r^2 value of 0.93 and a Spearman's Rho coefficient of 0.68 ($p = 0.0014$) were obtained for the predicted versus observed values. This suggests that the catalyst model produces a statistically significant rank ordering

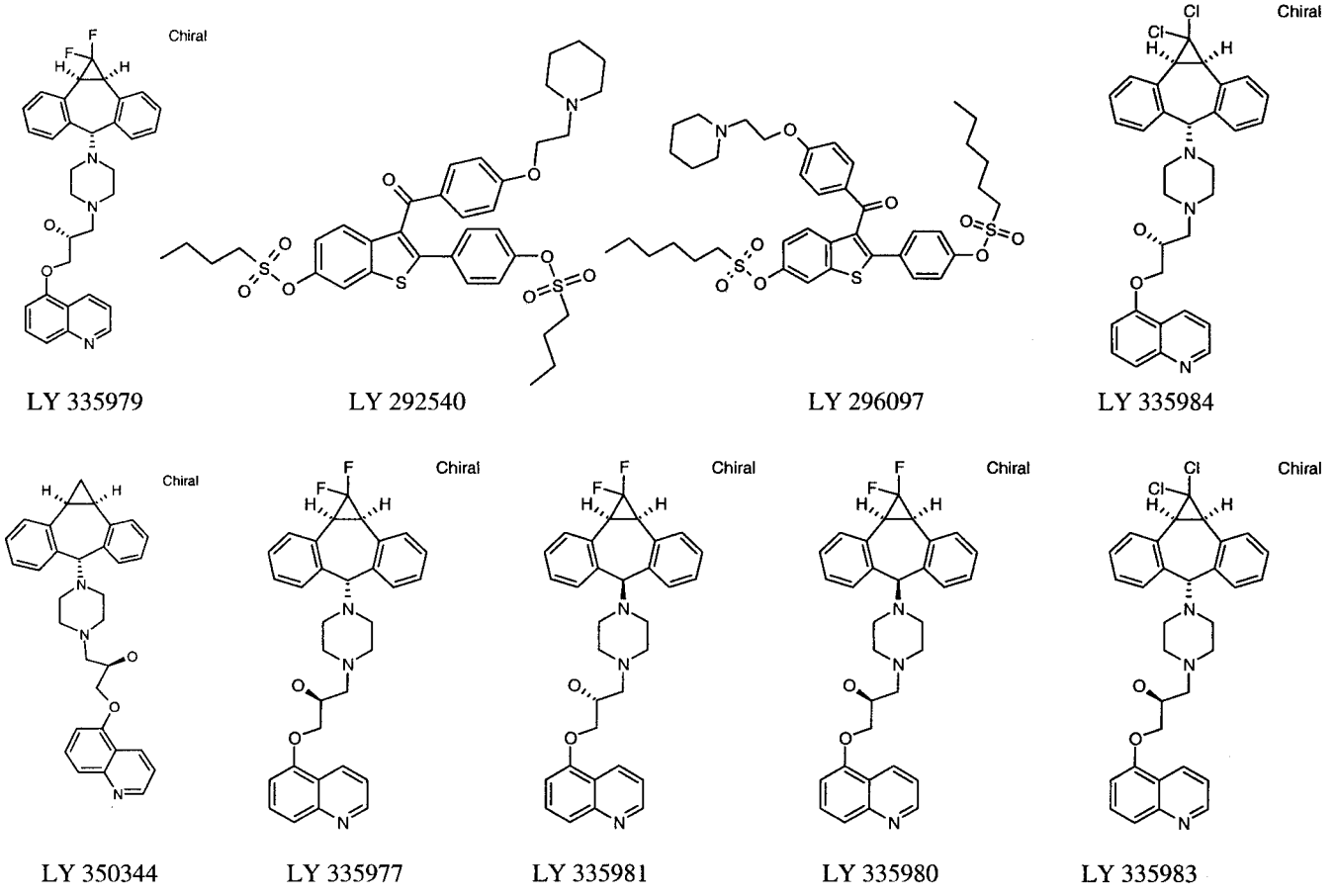

Fig. 1. Molecules used for pharmacophore modeling with an LY number.

of the test set molecules and that the model has value in predicting this external IC_{50} data. A third data set from inhibition of vinblastine accumulation in L-MDR-1 cells was predicted with the digoxin pharmacophore (Table 4). Seven molecules were predicted outside the log unit cut-off criteria, including ergometrine, dihydroergotamine, ergocornine, ergocristine, ergotamine, dihydroergocristine, and dihydroergocryptine. Besides these poor predictions, the correlation of observed and predicted data resulted in an r^2 value of 0.79 and a Spearman's Rho coefficient of 0.58 ($p = 0.017$), suggesting statistical significance in this models ability to predict inhibition of vinblastine accumulation. When calcein accumulation was evaluated in L-MDR-1 cells with the same pharmacophore (Table 5), 12 of 17 molecules were predicted outside the log unit cut-off. Consequently, there was a poor correlation of observed and predicted inhibition as an r^2 value of 0.41 and a nonsignificant Spearman's Rho coefficient of 0.3 ($p = 0.24$) resulted.

The second P-gp pharmacophore model was generated with the 21 molecules for inhibition of vinblastine binding (Table 3). The model yielded a pharmacophore with four features: three ring aromatic (five- and six-member aromatic rings) and one hydrophobic feature (Fig. 4) and an observed versus predicted correlation r^2 value of 0.88. The total energy cost of

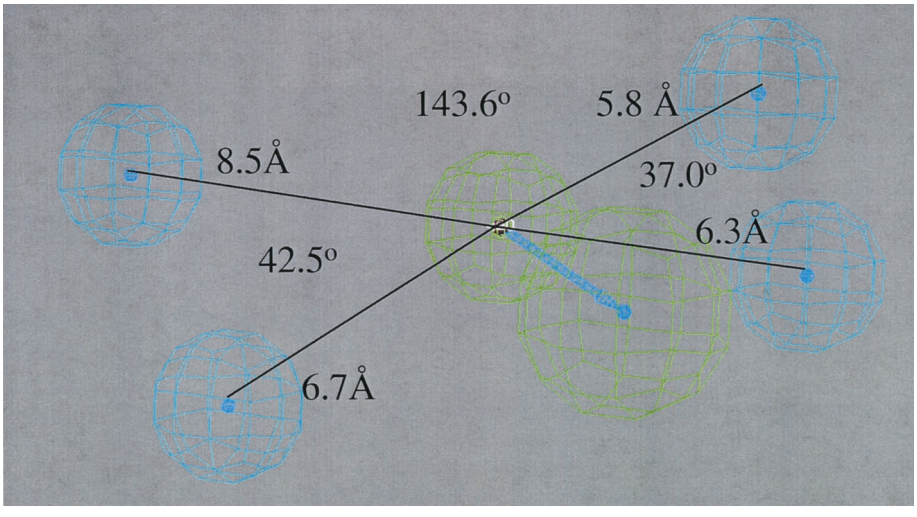

Fig. 2. The inhibition of digoxin transport P-gp pharmacophore (cyan, hydrophobe; green, hydrogen bond acceptor; arrow, vector).

TABLE 1
Inhibition of digoxin transport predictions using pharmacophore models

Molecule	Observed IC_{50} Digoxin Transport Model	Predicted IC_{50} Vinblastine Binding Model	Predicted K_I	
			Vinblastine Accumulation Model	Calcein Accumulation Model
		μM		
Caffeine	>100	1,700	1,200	19,000
S-Mephenytoin	>100	70	960	410
Tolbutamide	>100	8.9	9.9	410
Chlorzoxazone	>100	1,700	36	25,000
Morphine	>100	660	220	770
Alfentanil[a]	112	8.4	35	400
Debrisoquine	>100	1,700	82	4,500
Sufentanil[a]	4.2	0.78	40	400
Fexofenadine	>100	0.22	3.5	25
Fentanyl[a]	6.5	0.57	60	400
Loperamide[a]	2.7	2.1	2.7	85
CP 69042	2.3	6.1	25	49
Indinavir	44	4.4	27	28
Quinidine[b]	2.2	8.3	29	180
Nelfinavir	1.4	2.6	37	360
Saquinavir	6.5	3.4	3.7	33
Verapamil[b]	2.1	—[c]	0.84	7.9
Mibefradil	1.2	8.3	11	400
Ketoconazole	1.2	1.7	—[c]	—[c]
CP 12379[b]	0.7	0.37	22	19
CP 147478[b]	0.14	0.26	32	69
CP 114769[b]	0.3	0.12	15	7
CP 117227[b]	0.074	0.32	31	150
CP 101556[b]	0.6	0.24	2.7	8.5
LY335979	0.024	—[c]	29	400
CP 114416[b]	0.036	0.72	1.3	10
CP 100356[b]	0.114	0.45	1.4	4.3

[a] IC_{50} data presented as an abstract by Wandell et al. (1999a).
[b] IC_{50} data previously published in Wandell et al. (1999b).
[c] Molecule in training set.

this pharmacophore was 99.5 units, lower than the null cost (137.4 units). Permuting the activity and structures 10 times resulted in a lower mean r^2 value (0.31) for the training set; however, 3 of the 10 hypotheses could not generate a model.

The inhibition of vinblastine binding pharmacophore enabled visualization of important features on likely inhibitors (Fig. 5). The model predicts the inhibition of digoxin transport data (Table 1), although alfentanil, fexofenadine, fentanyl, and CP 114416 exceeded the log residual cutoff. Overall, the correlation for the observed versus predicted inhibition of vinblastine binding resulted in an r^2 value of 0.34 and a Spearman's Rho coefficient of 0.70 ($p = 0.0001$). This represents a statistically significant rank ordering of external data using this pharmacophore. Once again, verapamil and LY335979 were excluded from this evaluation because they were included in the training set. This pharmacophore did not, however, appropriately rank vinblastine accumulation (Table 4) or calcein accumulation data (Table 5), because seven and eight molecules, respectively, were predicted outside log residual cut-off. The Spearman's Rho rank for the observed versus predicted inhibition data resulted in nonsignificant coefficients of 0.05 and 0.1, respectively ($p > 0.05$).

A third P-gp model was generated from 17 inhibitors of vinblastine accumulation in L-MDR-1 cells (Table 4) and suggested a pharmacophore four hydrophobic features and one hydrogen bond acceptor feature (Fig. 6). This had an observed versus predicted correlation $r^2 = 0.86$ and total energy cost of 80 and null cost of 77.1 units. Permuting the activity and structures 10 times resulted in a lower mean r^2 value (0.64). Because LY335979 was not used in the training set, the highest affinity inhibitor, reserpine, was fitted to this pharmacophore (Fig. 7); it coincides with all the features. This model was found to predict inhibition of digoxin transport (Table 1) although 11 molecules were predicted outside the log residual cut-off. An r^2 value of 0.22 and Spearman's Rho coefficient for observed versus predicted inhibition of vinblastine accumulation of 0.46 ($p < 0.018$) was obtained. This pharmacophore did not, however, significantly rank the data for inhibition of vinblastine binding to plasma vesicles of CEM/VLB_{100} cells (Table 3) as the Spearman's Rho coefficient was 0.24 ($p > 0.05$).

A fourth P-gp model was generated from 18 inhibitors of calcein accumulation in L-MDR-1 cells (Table 5) and suggested a pharmacophore 2 hydrophobic features, one hydrogen bond acceptor, and 1 hydrogen bond donor feature (Fig. 8). This model possessed a correlation of observed and predicted inhibition with an r^2 value of 0.76 and total energy cost of 86.5 and null cost of 86.9 units. Permuting the activity and structures 10 times resulted in a lower mean r^2 value (0.56). The highest affinity inhibitor, bromocriptine, was fitted to this pharmacophore (Fig. 9) and found to coincide with all the pharmacophore features. This model was found to predict inhibition of digoxin transport (Table 1), although 15 molecules were predicted outside the log unit cut-off. The Spearman's Rho for observed versus predicted values resulted in a coefficient of 0.59 ($p < 0.0011$). This pharmacophore did not significantly rank the data for inhibition of vinblastine binding to plasma vesicles of CEM/VLB_{100} cells (Table 3) because the Spearman Rho coefficient was 0.32 ($p > 0.05$). The vinblastine accumulation data was not used with this calcein model because it contained identical molecules.

Discussion

In recent years, the complexity of transport by and modulation of P-gp has been described by many groups (Borgnia et al., 1996; Chiba et al., 1996; Klopman et al., 1997; Pajeva and Wiese, 1997, 1998a,b; Salem et al., 1998; Tmej et al., 1998; Bakken and Jurs, 2000). This complexity alone suggests that it would be a very difficult target for computational modeling. Traditionally, these models for P-gp inhibition were based around large numbers of structurally similar analogs known to be inhibitors, such as phenothiazones (Pajeva and Wiese, 1997), propafenone inhibitors (Pajeva and Wiese, 1998b), or diverse inhibitors of its ATPase activity (Osterberg and Norinder, 2000). To date, computational modeling of P-gp integrating its proposed multiple binding sites has not been described. In the present study, using structurally divergent P-gp inhibitors and probe P-gp substrates, we have been able to generate four distinct 3D-QSAR models that contain hydrogen bond acceptors, hydrogen bond donors, hydrophobes, and ring aromatic features. Some models seem to rank-order the data in the other sets, possibly indicating partial overlap for the binding sites probed by digoxin and vinblastine. Mod-

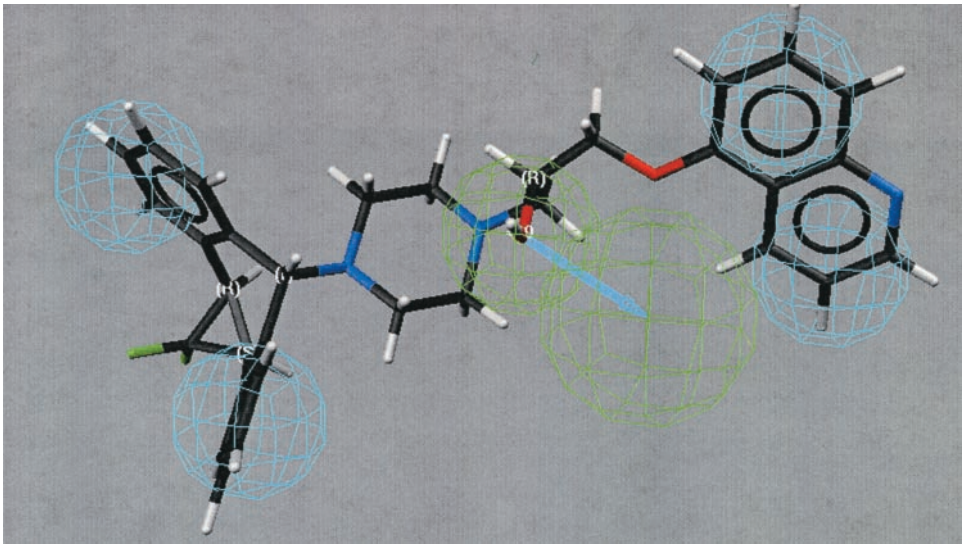

Fig. 3. LY335979 fast fit to the inhibition of digoxin transport P-gp pharmacophore (cyan, hydrophobe; green, hydrogen bond acceptor; arrow, vector).

els using data for inhibition of vinblastine accumulation and vinblastine binding in different systems do not predict each other completely. The vinblastine binding or digoxin transport models do not rank calcein accumulation data to a statistically significant extent. These different results may be indicative of some of the caveats of each respective in vitro system in that the assays for accumulation of substrates (vinblastine and calcein) involve the inhibitors crossing the membrane of the LLC-PK1 cells and then presumably binding at unspecified sites within the cells. This is mechanistically different from inhibition of vinblastine binding to plasma vesicles of CEM/VLB_{100} cells because the inhibitors are required solely to interfere with binding. The data derived with calcein and LLC-PK1 cells may also indicate that it is binding a separate site; however, the pharmacophore built with calcein data is able to rank the digoxin transport data, possibly suggesting some degree of overlap.

The catalyst model built with 27 inhibitors of digoxin transport by P-gp seems to represent the most useful predictive model for both molecules known to inhibit digoxin transport or vinblastine binding. This model contains one of the most potent inhibitors of P-gp previously reported, LY335979 [IC_{50}, 0.059 μM (Dantzig et al., 1996)], which fits well to the model (Fig. 3) indicative that this may have potential in designing molecules with similar or greater affinity that fit this pharmacophore. In the case of the vinblastine inhibition pharmacophore, this was less predictive for the digoxin data as judged by the r^2 value; however, the Spearman's Rho coefficient suggested that both models are equivalent (0.68

TABLE 2.
Inhibition of digoxin transport test set predicted using inhibition of digoxin transport pharmacophore.

Molecule	IC_{50}	
	Observed	Predicted
	μM	
Fluoxetine	>10	220
Procainamide	>10	37
Ivermectin	>10	3.1
Lovastatin	<10	7.5
Tamoxifen	10–100	13
Midazolam	10–100	28
Cortisol	10–100	38
Terfenadine	<10	6.9
Erythromycin	10	9.2
FK506[a]	0.74	10
Cyclosporin[a]	1.3	0.9
Ritonavir	3.8	2
PSC833[a]	0.11	2.3
Mitomycin C	>10	220
Colchicine	>100	7.3
Daunomycin	10–100	6.9
Paclitaxel	>100	32
Vinblastine	<10	6.3
CP 99542[a]	3.8	0.84

[a] IC_{50} data previously published in Wandell et al. (1999a).

TABLE 3
Inhibition of vinblastine binding predictions using pharmacophore models

Molecule	Observed IC_{50} Vinblastine Binding Model	Predicted IC_{50} Digoxin Transport Model	Predicted K_I	
			Vinblastine Accumulation Model	Calcein Accumulation Model
	μM		μM	
Verapamil	22.6	—[a]	0.84	7.9
Vinblastine	6	6.3	26	280
Vincristine	15	9.4	62	410
Actinomycin D	17	0.46	9.1	5
Etoposide	6	6.8	22	230
Paclitaxel	24	32	45	410
LY311306	1	0.74	19	19
Mitomycin C	>400	220	930	700
Doxorubicn	72	6.8	37	400
Colchicine	89	7.3	35	1000
TMBY (LY209662)	3.2	1	1.1	56
LY292540	4	0.62	14	15
LY296097	1.5	0.48	2.8	11
GF 120918	0.009	0.49	1.1	10
LY335984	0.053	0.31	27	33
LY350344	0.12	0.99	40	400
LY335977	0.29	0.84	36	400
LY335981	0.33	2.2	32	400
LY335980	0.25	1.4	25	400
LY335979	0.059	—[a]	29	400
LY335983	0.12	0.51	40	400

[a] Molecule in the training set.

TABLE 4
Inhibition of vinblastine accumulation predictions using pharmacophore models

Molecule	Observed K_I Vinblastine Accumulation Model	Predicted IC_{50}	
		Digoxin Transport Model	Vinblastine Binding Model
	μM	μM	
Ergometrine	100	8.3	8.3
Troleandomycin	87.64	11	1700
Clotrimazole	29.92	74	10
Erythromycin	37.79	7.9	1700
Fluconazole	400	230	8.4
Ketoconazole	5.27	6.7	2.6
Miconazole	26.36	8.4	0.31
Reserpine	0.97	1.1	8.3
Dihydroergotamine	119.94	1.6	3.8
Ergocornine	24.5	0.64	8.6
Ergocristine	13.33	0.58	8.4
Ergotamine	14.25	1.2	8.3
Bromocriptine	3.96	3.5	8.4
Ergocryptine	6.43	1.9	8.4
Dihydroergocristine	16	0.95	8.3
Dihydroergocryptine	19.82	0.36	8.4
Cyclosporin	1.3	0.9	1700

TABLE 5
Inhibition of calcein accumulation predictions using pharmacophore models

Molecule	Observed K_I Calcein Accumulation Model	Predicted IC_{50}	
		Digoxin Transport Model	Vinblastine Binding Model
	μM	μM	
Ergometrine	115.5	8.3	8.3
Troleandomycin	483.3	11	1700
Amiodarone	5.78	0.44	0.33
Clotrimazole	44	74	10
Erythromycin	1000	7.9	1700
Fluconazole	1000	230	8.4
Ketoconazole	24.9	6.7	2.6
Miconazole	55.5	8.4	0.31
Reserpine	12.2	1.1	8.3
Dihydroergotamine	1000	1.6	3.8
Ergocornine	105.2	0.64	8.6
Ergocristine	42.8	0.58	8.4
Ergotamine	98.9	1.2	8.3
Bromocriptine	2.81	3.5	8.4
Ergocryptine	12.2	1.9	8.4
Dihydroergocristine	511	0.95	8.3
Dihydroergocryptine	360.5	0.36	8.4
Cyclosporin	4.66	0.9	1700

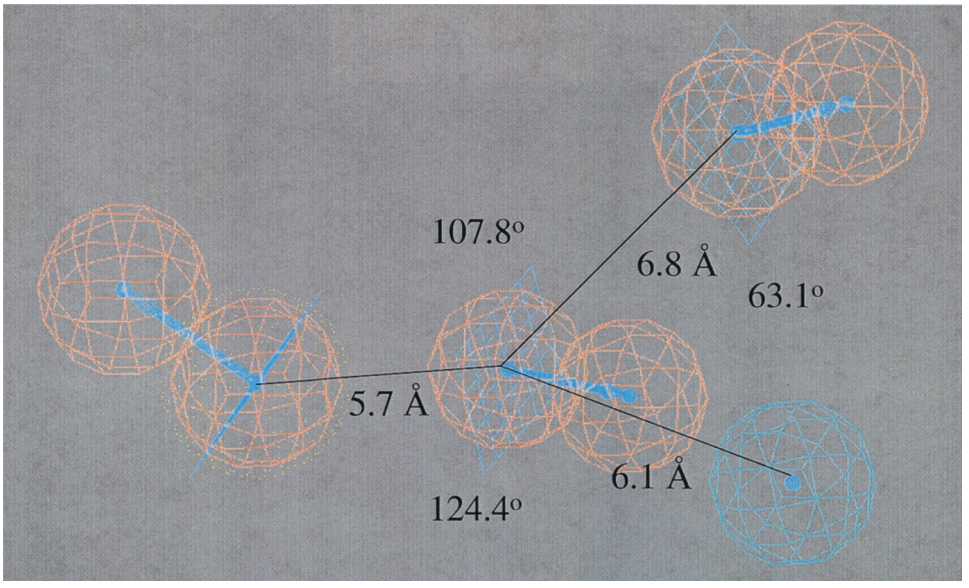

Fig. 4. The inhibition of vinblastine transport P-gp pharmacophore showing features and distances (orange, ring aromatic features; cyan, hydrophobic feature).

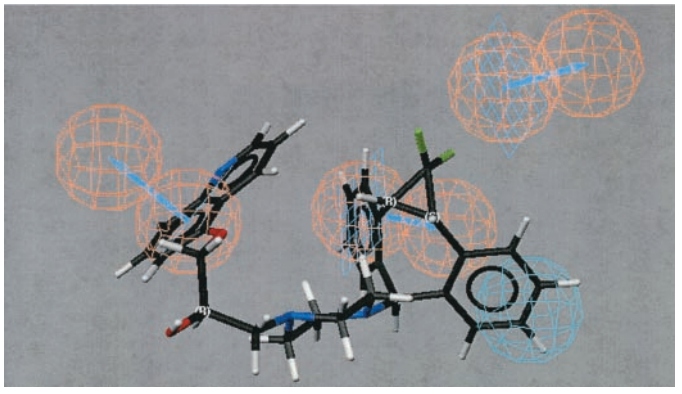

Fig. 5. LY335979 fitted to the inhibition of vinblastine transport P-gp pharmacophore features (orange, ring aromatic features; cyan, hydrophobic feature).

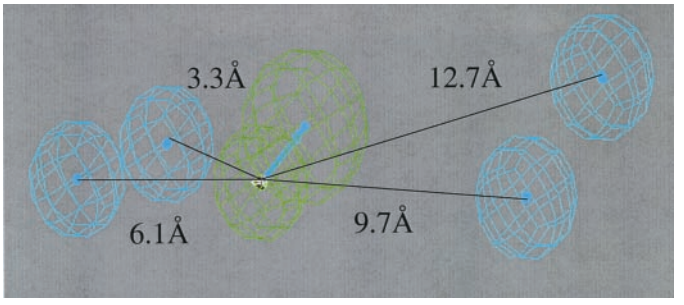

Fig. 6. Inhibition of vinblastine accumulation P-gp pharmacophore (green, hydrogen bond acceptor; cyan, hydrophobic features).

and 0.70) at ranking the compounds in the other training set. The vinblastine and calcein accumulation pharmacophores seem to be less valuable at predicting the other data sets based on the Spearman's Rho ranking statistics, the small energy difference between null and final pharmacophores, and the slight change in this value after permuting. Overall, this lesser success with these two models may be a consequence of the limited structural diversity of these two training sets, producing pharmacophores that explain less of the P-gp binding site(s).

Therefore, to some extent, the four catalyst models produced in this study allow visualization of the inhibitors and their respective fit that may correspond to regions on the P-gp protein. Such computational models can be clearly applied to order compounds for P-gp inhibition and may have utility in future drug design, although clearly those models based on more molecule classes have a greater success in this regard. Although a number of data sets for P-gp inhibition exist, few 3D-QSAR computational models have been published relating to diverse inhibitors of P-gp. Moreover, to our knowledge, no study has used such a structurally diverse training set of inhibitors for a single site of P-gp.

When these four models are assessed together, the features possessed by all models seem to agree with the previous publications in terms of the importance of hydrogen bonding and hydrophobicity (Osterberg and Norinder, 2000). Indeed, our models all contain at least one hydrophobic feature that could represent aliphatic or aromatic hydrophobes. The initial P-gp pharmacophore suggested in 1989 (Pearce et al., 1989) consisting of aromatic rings and a basic nitrogen atom can be extended by the pharmacophores described in this present study. In all cases based on this present study, the pharmacophores for P-gp inhibitors would seem to be quite large.

In conclusion, the cocorrelations for vinblastine binding and digoxin transport by P-gp at the very least suggest they share or represent the same binding site. It is likely that the calcein binding site also partially overlaps with these same molecules because the model derived from this data was able to rank the inhibition of digoxin transport by P-gp data. However, the poor correlation observed between models for inhibition of vinblastine binding to plasma vesicles of CEM/VLB_{100} cells and vinblastine accumulation in LLC-PK1 cells is probably a result of the differing complexities of each in vitro system rather than a reflection of separate sites being involved in binding and transport of this P-gp substrate. We may have defined pharmacophores for what could be interpreted as multiple regions within the same binding site of P-gp as probed by the particular substrates. This hypothesis is based on each pharmacophore being slightly different in its feature content, angles, and distances. However, these differences may also be related to the structural diversity of

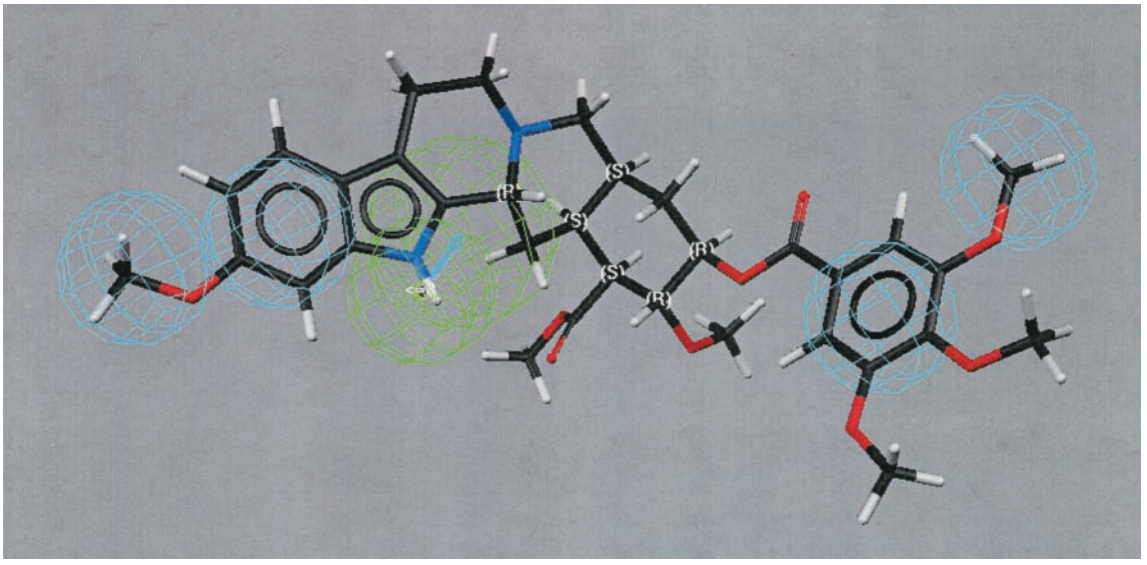

Fig. 7. Reserpine fitted to the inhibition of vinblastine accumulation P-gp pharmacophore (green, hydrogen bond acceptor; cyan, hydrophobic features).

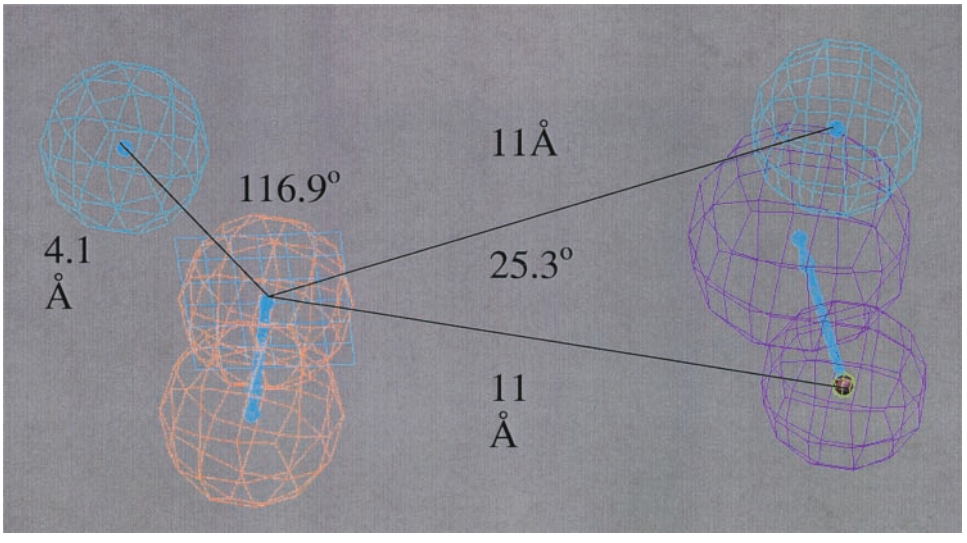

Fig. 8. Inhibition of calcein accumulation P-gp pharmacophore (orange, ring aromatic feature; purple, hydrogen bond donor; cyan, hydrophobic features).

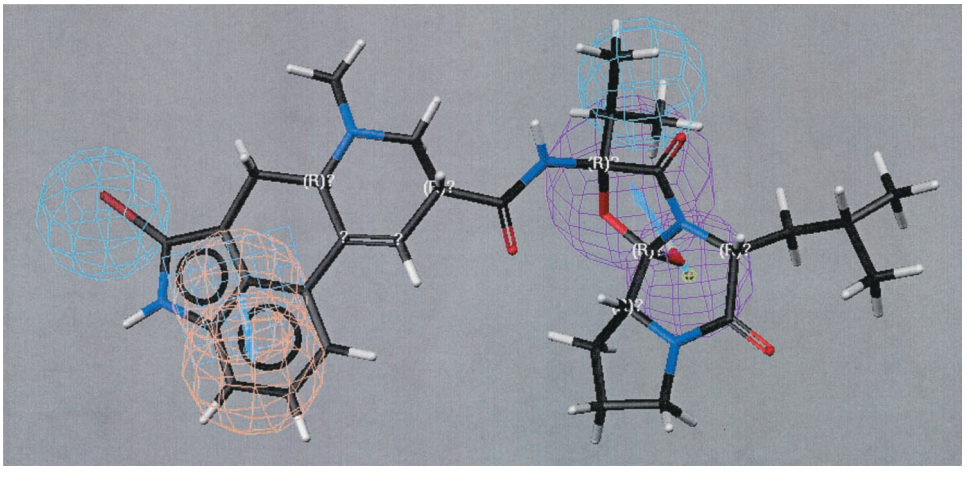

Fig. 9. Bromocriptine fitted to the inhibition of calcein accumulation P-gp pharmacophore (orange, ring aromatic feature; purple, hydrogen bond donor; cyan, hydrophobic features).

molecules in each training set and the use of IC_{50} values in most cases, which presents certain caveats in the interpretation of this data. Naturally, K_i values relate more closely to competitive inhibitors and a true binding affinity for P-gp and would be the ideal measure for generating such models, the cross-predictivity of most data sets in this study provides us with a means of model validation between IC_{50} and K_i. Future studies incorporating additional P-gp probes may de-

fine other binding sites or aid in the generation of more detailed pharmacophores described in this study. In addition, the enhancement and availability of detailed P-gp pharmacophore models may prove valuable for both drug discovery and screening.

Acknowledgments

We gratefully acknowledge Dr. Kate Hillgren for comments on this manuscript.

References

Ayesh S, Shao Y-M, and Stein WD (1996) Co-operative, competitive and non-competitive interactions between modulators of P-glycoprotein. *Biochimica et Biophysica Acta* **1316:**8–18.

Bakken GA and Jurs PC (2000) Classification of multidrug-resistance reversal agents using structure-based descriptors and linear discriminant analysis. *J Med Chem* **43:**4534–4541.

Borgnia MJ, Eytan GD, and Assaraf YG (1996) Competition of hydrophobic peptides, cytotoxic drugs, and chemosensitizers on a common P-glycoprotein pharmacophore as revealed by its ATPase activity. *J Biol Chem* **271:**3163–3171.

Chiba P, Ecker G, Schmid D, Drach J, Tell B, Goldenberg S, and Gekeler V (1996) Structural requirements for activity of propafenone-type modulators in P-glycoprotein-mediated multidrug resistance. *Mol Pharmacol* **49:**1122–1130.

Dantzig AH, Shephard RL, Cao J, Law KL, Ehlhardt WJ, Baughman TM, Bumol TF, and Starling JJ (1996) Reversal of P-glycoprotein-mediated multidrug resistaance by a potent cyclopropyldibenzosuberane modulator, LY335979. *Cancer Res* **56:** 4171–4179.

Demeule M, Laplante A, Murphy GF, Wenger RM, and Beliveau R (1998) Identification of the cyclosporin-binding site in P-glycoprotein. *Biochemistry* **37:**18110–18118.

Dey S, Ramachandra M, Pastan I, Gottesman MM, and Ambudkar S (1997) Evidence for two nonidentical drug-interaction sites in the human P-glycoprotein. *Proc Natl Acad Sci USA* **94:**10594–10599.

Ecker G, Huber M, Schmid D, and Chiba P (1999) The importance of a nitrogen atom in modulators of multidrug resistance. *Mol Pharmacol* **56:**791–796.

Ekins S, Bravi G, Binkley S, Gillespie JS, Ring BJ, Wikel JH, and Wrighton SA (1999) Three dimensional-quantitative structure activity relationship (3D-QSAR) analyses of inhibitors for CYP3A4. *J Pharmacol Exp Ther* **290:**429–438.

Ekins S, Ring BJ, Bravi G, Wikel JH, and Wrighton SA (2000) Predicting drug-drug interactions in silico using pharmacophores: A paradigm for the next millennium, in *Pharmacophore, Perception, Development, and Use in Drug Design* (Guner OF ed) pp 269–299, University International Line, San Diego.

Hoffmeyer S, Burk O, von Richter O, Arnold HP, Brockmoller J, Johne A, Cascorbi I, Gerloff T, Roots I, Eichelbaum M, et al. (2000) Functional polymorphisms of the human multidrug-resistance gene: multiple sequence variations and correlation of one allele with P-glycoprotein expression and activity in vivo. *Proc Natl Acad Sci USA* **97:**3473–3478.

Kim R, Fromm MF, Wandel C, Leake B, Wood AJ, Roden DM, and Wilkinson GR (1998) The drug transporter P-glycoprotein limits oral absorption and brain entry of HIV-1 protease inhibitors. *J Clin Invest* **101:**289–294.

Klopman G, Leming MS, and Ramu A (1997) Quantitative structure-activity relationship of multidrug resistance reversal agents. *J Pharmacol Exp Ther* **52:**323–334.

Lan LB, Ayesh S, Lyubinov E, Pashinsky I, and Stein WD (1996) Kinetic parameters for reversal of the multidrug pump as measured for drug accumulation and cell killing. *Cancer Chemother Pharmacol* **38:**181–190.

Lever JE (1977) Active amino acid transport in plasma membrane vesicles from Simian virus 40-transformed mouse fibroblasts. Characteristics of electrochemical Na^+ gradient-stimulated uptake. *J Biol Chem* **252:**1990–1997.

Neuhoff S, Langguth P, Dressler C, Andersson TB, Regardh CG, and Spahn-Langguth H (2000) Affinities at the verapamil binding site of MDR1-encoded P-glycoprotein: drugs and analogs, stereoisomers and metabolites. *Int J Clin Pharmacol Ther* **38:**168–179.

Osterberg T and Norinder U (2000) Theoretical calculation and prediction of P-glycoprotein-interacting drugs using MolSurf parameterization and PLS statistics. *Eur J Pharm Sci* **10:**295–303.

Pajeva I and Wiese M (1998a) Molecular modeling of phenothiazines and related drugs as multidrug resistance modifiers: a comparative molecular field analysis study. *J Med Chem* **41:**1815–1826.

Pajeva IK and Wiese M (1997) QSAR and molecular modelling of catamphiphilic drugs able to modulate multidrug resistance in tumors. *QSAR* **16:**1–10.

Pajeva IK and Wiese M (1998b) A comparitive molecular field analysis of propafenone-type modulators of cancer multidrug resistance. *QSAR* **17:**301–312.

Pearce HL, Safa AR, Bach NJ, Winter MA, Cirtain MC, and Beck WT (1989) Essential features of the P-glycoprotein pharmacophore as defined by a series of reserpine analogs that modulate multidrug resistance. *Proc Natl Acad Sci USA* **86:**5182–51332.

Pearce HL, Winter MA, and Beck WT (1990) Structural characteristics of compounds that modulate P-glycoprotein-associated multidrug resistance. *Adv Enzyme Regul* **30:**357–373.

Ramu A and Ramu N (1992) Reversal of multidrug resistance by phenothiazines and structurally related compounds. *Cancer Chemother Pharmacol* **30:**165–173.

Salem M, Richter E, Hitzler M, Chiba P, and Ecker G (1998) Studies on propafenone-type modulators of multidrug resistance VIII: synthesis and pharmacological activity of indanon analogues. *Sci Pharm* **66:**147–158.

Scala S, Akhmed N, Rao US, Paull K, Lan L-B, Dickstein B, Lee J-S, Elgemeie GH, Stein WD, and Bates SE (1997) P-glycoprotein substrates and antagonists cluster into two distinct groups. *Mol Pharmacol* **51:**1024–1033.

Schinkel AH, Wagenaar E, van Deemter L, Mol C, and Borst P (1995) Absence of the mdr1a p-glycoprotein in mice affects tissue distribution and pharmacokinetics of dexamethasone, digoxin and cyclosporin A. *J Clin Invest* **96:**1698–1705.

Schmid D, Ecker G, Kopp S, Hitzler M, and Chiba P (1999) Structure-activity relationship studies of propafenone analogs based on P-glycoprotein ATPase activity measurements. *Biochem Pharmacol* **58:**1447–1456.

Schuetz JD and Schuetz EG (1993) Extracellular matrix regulation of multidrug resistance in primary monolayer cultures of adult rat hepatocytes. *Cell Growth Differ* **4:**31–40.

Seelig A (1998) How does P-glycoprotein recognize its substrates? *Int J Clin Pharmacol Ther* **36:**50–54.

Shapiro AB and Ling V (1997) Positively cooperative sites for drug transport by P-glycoprotein with distinct drug specificities. *Eur J Biochem* **250:**130–137.

Shepard RL, Winter MA, Hsaio SC, Pearce HL, Beck WT, and Dantzig AH (1998) Effect of modulators on the ATPase activity and vanadate nucleotide trapping of human P-glycoprotein. *Biochem Pharmacol* **56:**719–727.

Smith PK, Krohn RI, Hermanson GT, Mallia AK, Gartner FH, Provenzano MD, Fujimoto EK, Goeke NM, Olson BJ, and Klenk DC (1985) Measurement of protein using bicinchoninic acid. *Anal Biochem* **150:**76–85.

Tiberghein F and Loor F (1996) Ranking of P-glycoprotein substrates and inhibitors by a calcein-AM fluorometry screening assay. *Anti-Cancer Drugs* **7:**568–578.

Tmej C, Chiba P, Huber M, Richter E, Hitzler M, Schaper K-J, and Ecker G (1998) A combined Hansch/free Wilson approach as predictive tool in QSAR studies on propafenone-type modulators of multidrug resistance. *Arch Pharm (Weinheim)* **331:**233–240.

Wandell C, Kim RB, Kajiji S, Guengerich FP, Wilkinson GR, and Wood AJJ (1999a) P-glycoprotein and cytochrome P-450 3A inhibition: dissociation of inhibitory potencies. *Cancer Res* **59:**3944–3948.

Wandell C, Kim RB, and Wood AJJ (1999b) Interaction between P-glycoprotein and opioids (Abstract). *Anesthesiology* **91:**A445.

Weininger D (1988) SMILES 1. Introduction and encoding rules. *J Chem Inf Comput Sci* **28:**31.

Address correspondence to: Sean Ekins, Ph.D., Concurrent Pharmaceuticals Inc., One Broadway, 14th Floor, Cambridge, MA 02142. E-mail: ekinssean@yahoo.com